

Compared influence of the Atlantic Multidecadal Variability and of spring soil moisture on summer heat waves in Europe

Valeria Mascolo^{1,+,*}, Clément Le Priol^{1,2,*}, Fabio D'Andrea², and Freddy Bouchet²

¹Laboratoire de Physique à l'ENS de Lyon, CNRS, F-69342 Lyon, France

²Laboratoire de Météorologie Dynamique, IPSL, ENS-PSL, CNRS, Paris, France

⁺Corresponding author: valeria.mascolo@ens-lyon.fr

^{*}Authors contributed equally to the article.

Abstract

In this work, we study and compare the influence of the Atlantic Multidecadal Variability (AMV) and of spring soil moisture in Southern Europe on the duration and intensity of European summer heat waves. We study common heat waves with return times of a few years like in previous studies, but we also propose a new methodological approach, *return time maps*, that allows us to study rare heat waves with return times from 10 to 50 years.

We use the outputs from three climate models, namely IPSL-CM6A-LR, EC-Earth3, and CNRM-CM6-1, in which North Atlantic sea surface temperatures are restored towards the observed AMV anomalies. The three models give consistent results, with the exception of EC-Earth simulating a much greater influence of soil moisture.

Typical AMV or spring soil moisture anomalies induce changes in the temperature and duration of heat waves that are of comparable amplitude, but follow different regional patterns. As might be expected, a positive AMV phase or low soil moisture induces hotter and longer typical heat waves over most of Europe. However, counter-intuitively, they also induce less heat wave days and cooler heat waves over part of Northeast Europe.

For more extreme events, the influence of the AMV and soil moisture increase, according to rather similar regional patterns as for typical heat waves. However, while the amplitude of the influence is greater, the regions with decreased heat wave temperature and less heat wave days extend in size.

Lay Summary Beyond the daily fluctuations of the weather, the occurrence and intensity of heat waves can be modulated by slow drivers. In this work, we study and compare the influence of two slow drivers on the duration and intensity of summer heat waves in Europe. The first driver is a slow mode of variation of the North Atlantic Ocean sea surface temperature which is called the Atlantic Multidecadal Variability (AMV). The second one is the quantity of water available in the soil in Southern Europe.

We study typical heat waves that occur almost every year, but we also introduce a new method to study rare heat waves that occur only every 10 or 50 years, on average.

Using results from global climate model experiments, we find that these two drivers have influences of comparable amplitudes on the duration and temperature of European summer heat waves. However, their influence follow different regional patterns.

1 Introduction

In a changing climate, extreme hot events are becoming more frequent and intense [1]. The impacts of those events are detrimental at many scales, causing damages to our society, environment, and other living being [2].

Europe, and especially the Mediterranean basin, are identified as a hot-spot for extreme hot events, with magnitude changing according to the future climate scenarios ([3] and references therein). In particular, heat extremes in Western Europe have warmed at a faster pace than elsewhere in the mid-latitudes [4].

Besides global warming, different physical drivers influence the formation of heat waves [5,6], acting on different timescales. Heat waves being linked to synoptic systems, the shorter timescale is the one of atmospheric variability [7,8], corresponding to a few days. Slower drivers are the soil moisture, which acts on a seasonal timescale, and slow modes of internal variability of the climates, acting on yearly to multidecadal timescales. These slow drivers can modulate the occurrence and frequency of heat waves [5]. The deficit of soil moisture at the beginning of summer in Southern Europe and the Atlantic Multidecadal Variability (AMV) are two slow drivers of particular importance in Europe.

Soil moisture deficit in the Mediterranean basin at the beginning of summer has proved to act as a precondition for some extreme events such as droughts [9,10] and heat waves [11–14] over continental Europe. The mechanism is the following. Dry and warm air masses form over the dry soils of the Mediterranean and induce diminished cloudiness. These air masses are advected northward by southerly wind episodes, increasing temperature and evaporative demand over Europe, which in turn conduces to drier soils. These drier soils amplify the warming through higher sensible heat emissions and favored upper-air anticyclonic circulation [10].

In addition, decadal variability of the sea surface temperature of the North Atlantic ocean has proven to influence the duration of heat waves in Europe [15–17] and to play a role on the occurrence of other extremes, such as droughts and precipitations in other parts of the globe [18–20]. This internally-driven low-frequency variation is known in the literature as the Atlantic Multidecadal Variability (AMV). Based on GCM studies, the Atlantic Meridional Overturning Circulation (AMOC) has been identified as a driver for the AMV [21–23]. On the atmospheric side, recent studies underlined how persistent North Atlantic Oscillation (NAO), considered to be the predominant mode of variability in the atmosphere in the Atlantic sector [24], could influence the thermohaline circulation and thus the AMV [25].

Our study aims at establishing which slow driver between the soil moisture and the AMV has the strongest influence on the occurrence and intensity of heat waves in Europe. Both typical heat waves and extreme ones, in term of probability, are analysed.

Indeed, previous studies [16,17] focused on common European heat waves, occurring every one or two years.

However, the most harmful events are the largest and rarest ones [26]. This calls for new methodologies for studying this sort of events. In this paper, we propose a new tool, *return time maps*, to study the influence of the AMV and spring soil moisture on extreme European summer heat waves.

We use two definitions of heat waves, which are complementary. The first one measures the number of heat wave days per year, based on the exceedance of two temperature thresholds [17,27]. However, it does not give any information on the intensity of the events. Thus we employ a second, complementary, definition where we fix the duration of the events studied and measure their intensity, characterized by the mean temperature anomaly during the event.

The paper is organized as follows. In section 2 we present the data used for this study and the two definitions of heat waves we use. In section 3 we compare the effects of the AMV and of soil moisture on common heat waves. In section 4 we introduce a methodology to study rare events with return times of a few decades and we assess which driver, between the AMV and spring soil moisture, has the strongest influence on these rare heat waves. We summarise our findings in section 5.

2 Data and methods

In this section we present the data used for this study and the methodology to fairly compare the influence of the AMV and of the soil moisture on heat waves in an independent way. We then introduce the two different heat wave definitions that we use for this study.

2.1 Data

2.1.1 DCP-AMV experiments

Given the relevance of the effects of the AMV on the climate and the potential predictability associated to it, there is ongoing work in both deepening the understanding of its dynamical drivers and in improving its representation in models. As we already pointed out in section 1, a source of the uncertainty of the effects of the AMV comes from the lack of fully understanding of the phenomenon itself. On top of that, model biases in representing crucial quantities for the AMV, such as the AMOC

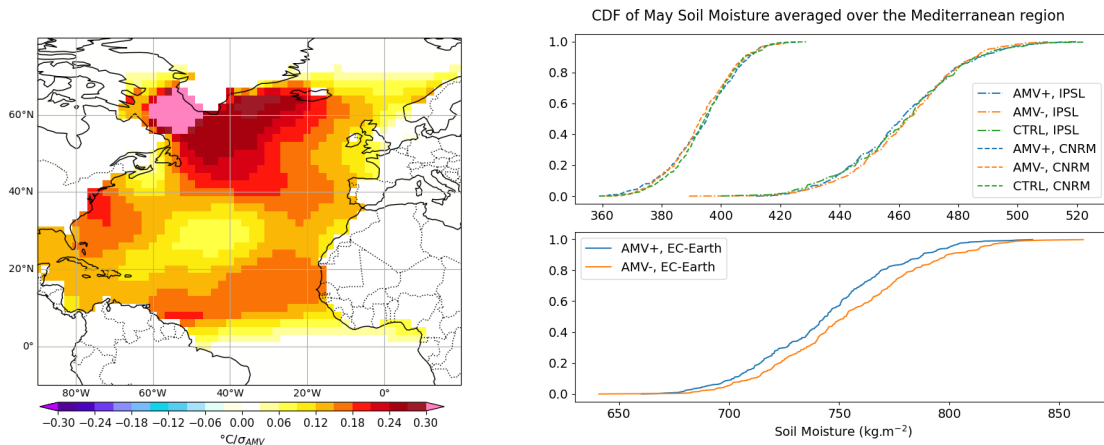


Figure 1: **Left:** SST anomaly pattern used for restoring the SST in the DCP-AMV experiments. Pattern courtesy C. Cassou. **Right:** Empirical cumulative density function of May soil moisture averaged over the Mediterranean region (35°N-46°N, 10°W-30°E) in each model (IPSL, CNRM, EC-Earth) and each experiment (AMV+,AMV-,CTRL).

and teleconnection patterns, contribute to the augmentation of this uncertainty. In this line of thought, it was showed in ref. [16] that CMIP5 models underestimate the coupling of ocean-atmosphere at low frequency. The importance of dedicated modeling protocols to study decadal variability, such as the AMV, both at a global and regional scale using a coordinated multi-model approach has also been underlined [23]. With this aim the Decadal Climate Prediction Project (DCPP) [28] part of the CMIP6 Project, was created.

Within the DCP, ensemble of simulations have been conducted to understand the predictability, variability and impacts of decadal modes of variability of the climate such as the AMV. We use the outputs of the DCP-C.1 experiments designed for enhancing the understanding of the impact of the AMV on the global climate. In these experiments, the sea surface temperature (SST) of the North-Atlantic is restored towards an anomalous SST pattern representative of the observed AMV, shown in fig. 1. The detailed procedure of the experiments can be found in the technical note of [28].

For the current study, we use the outputs from three coupled models that took part to the experiment: IPSL-CM6A-LR [29], EC-Earth3 [30] and CNRM-CM6-1 [31] (hereafter simply referred to as IPSL, EC-Earth and CNRM). Further details about the models can be found in appendix A and in the corresponding references. For each model AMV+ and AMV- ensembles consisting of many 10-year members have been computed. In the AMV+ ensemble, the SST is restored towards a positive anomaly pattern while in the AMV- it is restored towards its opposite. For IPSL and CNRM we also have a control run (CTRL) where the SST is nudged towards the climatology. The radiative forcing is set to its 1850 value. Table 1 summarizes the number of years available in each ensemble for each model.

To characterize the heat wave events we use the daily maximum 2 meter air temperature, while for the analysis of the soil moisture we use the total soil moisture integrated over the whole soil column (mrso). In section 3 and in appendix A we will show maps of other fields.

2.1.2 Observation-derived datasets for soil moisture

We use two observational datasets of land variables, ERA5-Land and GLEAM v3.8a, as a comparison for the persistence of soil moisture anomalies in the three models.

ERA5-Land [32] is a reanalysis dataset of land variables that describes the evolution of the water and energy cycles over land in a consistent manner. It goes back to 1950 and is produced through global high-resolution numerical integrations of the ECMWF land surface model driven by the downscaled meteorological forcing from the ERA5 climate reanalysis. We use monthly averaged of the volumetric soil water in the 4 soil layers of the model, corresponding to depth 0-289 cm. We chose to use the

Dataset \ Model	Model		
	IPSL	EC-Earth	CNRM
AMV+/-	500	320	390/400
CTRL	250	0	400
Dry/Wet	500	250	450

Table 1: *Number of years in all ensembles for each model.* The AMV+/- and CTRL ensembles consist of simulation members of 10 years. The Dry and Wet ensembles are built by sorting the years in all simulation members according to their average May Soil Moisture value over Southern Europe (see section 2.2 and appendix A for details). For CNRM, some surface air temperature and soil moisture outputs are missing.

weighted average over all the soil layers to perform a consistent analysis with the soil moisture used in the DCP data that we presented in the section above.

The Global Land Evaporation Amsterdam Model (GLEAM) is a set of algorithms dedicated to the estimation of terrestrial evaporation and root-zone soil moisture from satellite data [33, 34]. The surface soil moisture is assimilated from satellite microwave remote sensing data. The model features a multi-layer soil model driven by satellite observation of precipitation with fast and slow draining of the water from the surface layer towards the deepest layers. The soil moisture estimates are validated against 2325 soil moisture sensors across a broad range of ecosystems. We use GLEAM v3.8a monthly average datasets of the surface (0-10 cm depth) and root zone (10-100 cm) soil moisture. We perform the weighted average of the two datasets to obtain the soil moisture between 0 and 100 cm. GLEAM datasets run from 1980 to present.

2.2 Influence of the AMV on spring soil moisture and creation of the Dry and Wet ensembles

To assess the influence of spring soil moisture on summer heat waves we use the outputs of the three experiments (AMV+/- and CTRL), for each model, to build two new ensembles, called Dry and Wet, corresponding to low and high spring soil moisture, respectively. To this aim, we first compute the average May soil moisture SM_{av} for each year and each experiment over a domain covering Southern Europe. Following [9], we choose the extent of the domain to be the rectangular box 35°N-46°N, 10°W-30°E. Secondly, to rigorously compare the influence of soil moisture with the one of the AMV we must avoid an indirect influence of the AMV through soil moisture. To verify the influence of the AMV on SM_{av} in the models, we plot the cumulative density function (CDF) of SM_{av} on the right panel of fig. 1. The influence of a positive versus negative phase of the AMV on SM_{av} is negligible in IPSL and CNRM (-0.8 and $+0.6$ $kg.m^{-2}$ respectively, to be compared to standard deviations of 19.8 and 11.8 $kg.m^{-2}$) and relatively small in EC-Earth (-10.5 $kg.m^{-2}$ for a standard deviation of 34.4 $kg.m^{-2}$). To ensure that there is no indirect influence of the AMV at all, we constrain the number of years coming from the AMV+ and AMV- ensembles to be equal in the Dry and Wet ensembles.¹

The size of the Dry and Wet ensembles is such that the mean value of the soil moisture inside the Dry (resp. Wet) ensemble is nearly one standard deviation below (resp. above) the mean value of the soil moisture averaged over the AMV+/- and CTRL ensembles all-together. This makes the comparison with the AMV forcing meaningful because the targeted SST pattern for the relaxation corresponds to one standard deviation of the AMV variability.

Finally, we put years with low SM_{av} in the Dry ensemble and years with high SM_{av} in the Wet one. More details about the procedure to build the Dry and Wet ensembles can be found in appendix A.

2.3 Heat wave definitions

In this subsection we present the two definitions of heat waves used in this study. The first one comes from [27], and has been already successfully used in [20] and [17] to show the effect of the phase of the AMV on heat waves in North America and Europe respectively. It enables us to compare our results with the ones from [17], who has investigated the response to the AMV phase on heat waves in Europe

¹This constraint also enables us to deal with the imbalanced size of the AMV+/- ensembles of the CNRM model. Indeed, 120 years of soil moisture outputs are missing for the AMV- experiment with this model.

using earlier version of the CNRM and EC-Earth models. This first definition measure the number of heat wave days per year but does not give any information on the event’s intensity. In order to assess the influence of the slow drivers on heat waves intensities, we use a second, complementary, definition where we fix the duration of the heat waves and measure the corresponding temperature anomaly.

2.3.1 Threshold-based definition

We call the first definition that we use *threshold-based definition* as it relies on two temperature thresholds. According to this definition [17, 20, 27], an heat wave event is a group of days that satisfies the three following conditions:

- (i) T_{\max} must exceed T_1 for at least 3 consecutive days,
- (ii) T_{\max} averaged over the entire event must exceed T_1 and
- (iii) T_{\max} on each day of the event must exceed T_2 .

where T_{\max} is the daily maximum 2-meter air temperature and T_1 and T_2 are two temperature thresholds corresponding, respectively, to the 90th and 75th percentile of the local June-July-August (JJA) T_{\max} distribution built from the T_{\max} values of all members of the AMV+ and AMV- simulations (for each model). This definition is location-dependent, since the T_{\max} distribution varies with latitude and longitude. For each grid point, we count the number of heat wave days in each year. In this study we are interested at the response, in terms of heat wave days per year, to an AMV-forcing. We will first look at the mean difference between AMV+ and AMV- for each model in section 3 and then we condition on the most extreme years which have the highest number of heat wave days in section 4.

2.3.2 14-day heat waves

The threshold-based definition allows to measure the event duration based on daily temperature data, but it does not provide any information on the heat wave intensity. To quantify the heat wave intensities for several independent duration, heatwave indices based on the combined temporal and spatial averages of the surface or 2-meter temperature have been adopted in many studies. Notably, seminal studies of the 2003 Western European and 2010 Russian heat waves considered the averaged temperature over variable long time periods (7 days, 15 days, 1 month, and 3 months) [35–37]. Similar definitions have been adopted in a set of recent studies [38–43]. This viewpoint is expected to be complementary with more classical heat wave definitions [5] and extremely relevant to events with the most severe impacts.

The second definition that we use is the local seasonal maximum of the D -days average of the daily maximal temperature. Mathematically the definition reads as follows:

$$\tilde{A}(\mathbf{r}) = \max_{t, t+D \in \text{JJA}} \frac{1}{D} \int_t^{t+D} (T_{\max}(\mathbf{r}, t') - \bar{T}_{\max}(\mathbf{r})) dt', \quad (1)$$

where \mathbf{r} and t' are the spatial and time coordinates respectively. We do not perform any spatial average because we want to have a local view as with the threshold-based definition. To ease the comparison between different locations, we subtract $\bar{T}_{\max}(\mathbf{r})$, the local June-July-August (JJA) average of $T_{\max}(\mathbf{r}, t)$. We thus measure a temperature anomaly with respect to the local seasonal mean. We choose to focus on heat waves of duration $D = 14$ days and compute one value of \tilde{A} for each year and at each grid point.

3 Influence of the Atlantic Multidecadal Variability and of spring soil moisture on typical heat waves

In this section we compare the effect of the AMV and of spring soil moisture on typical heat waves. Following previous studies [17, 20], we first use the threshold-based definition introduced in section 2.3.1 to measure the drivers influence on the mean number of heat wave days per year. We then use our second definition, presented in section 2.3.2, to measure their influence on the 14-day heat wave intensity.

3.1 Influence on the frequency of heat wave days

In this section we study the effect of the AMV and spring soil moisture on heat waves using the threshold-based definition introduced in section 2.3.1. Figure 2 shows the difference in the mean number of heat wave days per year between the Dry and the Wet ensembles and the AMV+ and the AMV- ensembles for each of the three models. Both the AMV and spring soil moisture influence significantly the mean number of heat wave days over large areas of Europe. As could be expected, the influence of both the positive AMV phase and a reduced soil moisture is positive in most regions. However, there are also regions of small negative influence in Northeast Europe (between 0 and -1 heat wave days per year). They are located further North and East for the soil moisture conditioning compared to the AMV. Although the exact location is model dependent, such regions of negative influence are present in all models.

For the AMV, the region of largest influence is the Mediterranean basin² with positive differences from 1 to 3 heat wave days per year. These numbers must be compared with the mean number of heat wave days per year in the AMV- ensemble which is comprised between 7 and 10 heat wave days per year in most location (not shown). These results are in very good agreement with [17] where earlier versions of the CNRM and EC-Earth models were used (namely, CNRM-CM5 and EC-Earth3P).

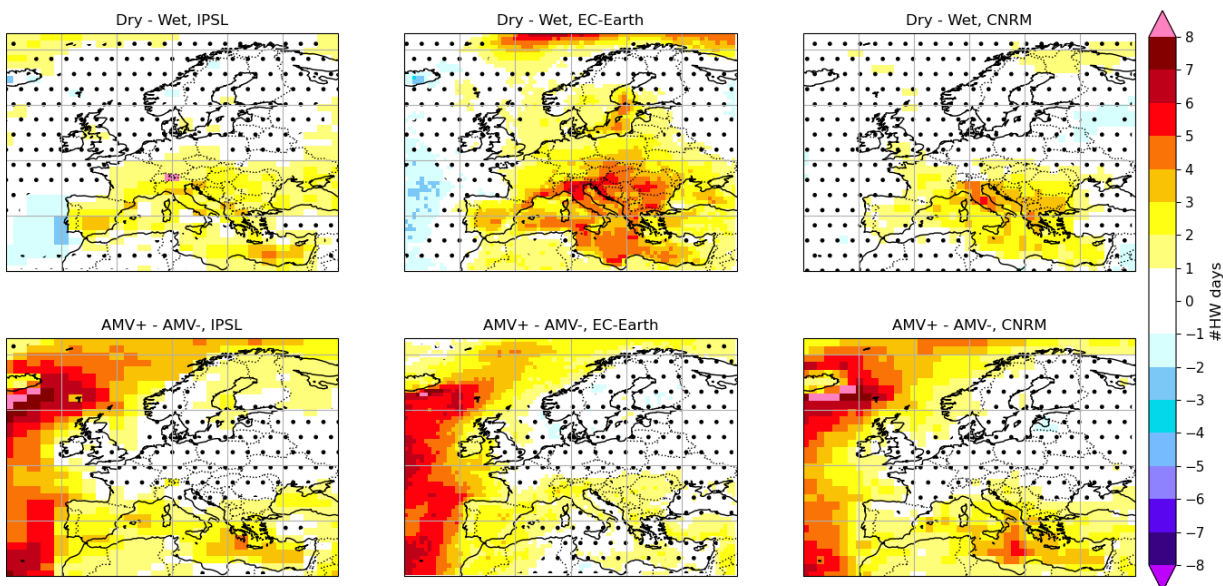


Figure 2: *Mean response maps for the frequency of heat wave days.* Differences in the mean number of heat wave days per year between the Dry and the Wet ensembles (top line) and the AMV+ and AMV- ensembles (bottom line) for each of the three models. Stippling denotes area below the 95% significance level according to a bootstrap test.

Regarding the influence of the soil moisture, the models present less consistent results. On the one hand, CNRM and IPSL show a positive response over Southern Europe which is mostly comprised between 1 and 3 heat wave days per year, and up to 4 heat wave days in some locations. In these two models the influence of soil moisture is thus slightly larger than the one of the AMV but still of comparable amplitude. On the other hand, EC-Earth simulates a much more extended and much larger positive influence of the soil moisture. The region of positive difference covers almost all Europe as well as Northern Africa with differences that range from 3 to 6 heat wave days per year over Spain, Italy and Southern Central Europe. In this model the soil moisture has a much stronger influence than the AMV.

Discrepancy between EC-Earth and the two other models. EC-Earth presents a drastically stronger response to spring soil moisture than the other two models. This stronger response is asso-

²We focus on land area only. The very large anomalies over the Atlantic ocean are due to the SST forcing of the simulations.

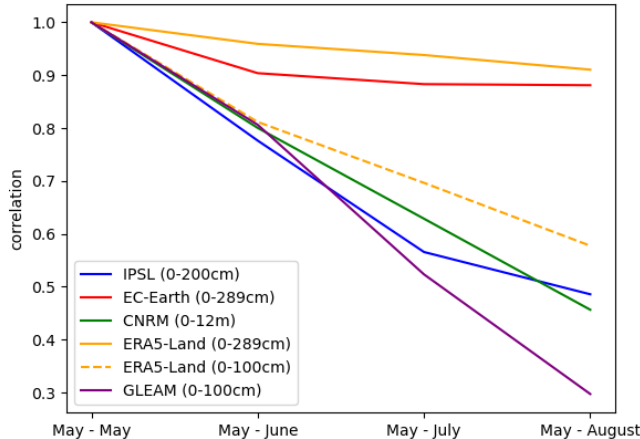


Figure 3: Pearson correlation coefficients between the month of May and the months of June, July, and August of the monthly averaged soil moisture averaged over Southern Europe (35°N - 46°N , 10°W - 30°E).

ciated to strong positive $Zg500$ anomaly and reduced precipitation over Central Europe (not shown). In order to further investigate the cause of this discrepancy, we show on fig. 3 the auto-correlation function of the monthly averaged soil moisture averaged over Southern Europe.

In IPSL and CNRM, the auto-correlation decays almost nearly from 1 for the May-May correlation to about 0.5 for May-August. On the other hand, in EC-Earth the correlation levels out for the three summer months and is nearly constant at about 0.9.

This larger correlation implies a stronger persistence of soil moisture anomalies in EC-Earth: dry soils in May remain abnormally dry throughout the summer, causing the surface air to heat up more strongly due to a larger sensible heat flux. We also plot for comparison the auto-correlation of the soil moisture in the observation-derived datasets ERA5-Land and GLEAM v3.8a. ERA5-Land shares the same land model, HTESSEL, with EC-Earth and also presents a strongly persistent auto-correlation of soil moisture. This indicates that the large correlation of EC-Earth is not due to an abnormal atmospheric response but rather to the land model itself. In an attempt to estimate if HTESSEL produces a too large auto-correlation of the soil moisture we compare the auto-correlation of the 1st meter of soil with GLEAM v3.8a, a product more directly derived from satellite observations than ERA5-Land. The auto-correlation for the months of July and August remains larger in ERA5-Land compared to GLEAM. Thus, it could be that HTESSEL produces too large persistence of soil moisture anomalies. However, it would be hasty to draw any definitive conclusions. While we consider the results of EC-Earth with some caution, we cannot rule it out.

3.2 Influence on the intensity of 14-day heat waves

We turn to the second definition to assess the influence of the AMV and spring soil moisture on the intensity of heat waves.

Figure 4 shows the mean difference in \tilde{A} (see section 2.3.2) between the Dry and Wet (top line) and AMV+ and AMV- (bottom line) ensembles. Note that these maps should not be interpreted as the temperature averaged on any given period of the summer. Indeed the 14 days that enter the average are a priori different for each grid point and for each year of the simulations. The patterns of influence are very similar to the ones observed in fig. 2 for heat wave duration. The influence of both factors over most parts of the continent is positive, but there are also regions of small negative influence in North-Eastern Europe.

The influence of the AMV concentrates on the Mediterranean Basin with positive differences ranging from 0.2 to 0.4°C in most places. All models predict influences of similar amplitude except in Northern Spain and Southern France where EC-Earth simulates higher differences, ranging from 0.5 to 0.8°C.

The influence of low soil moisture is largest in Southern Europe. For CNRM and IPSL it has a

peak amplitude which is slightly higher than the one of the AMV with differences going up to 0.5 or 0.6°C in many locations. As for heat wave duration, EC-Earth simulates a much larger influence of low soil moisture with positive differences above 0.8°C over all Western and Central Europe and peak differences up to 1.3°C over the Balkans. As for the first definition, we expect the stronger Dry-Wet response of EC-Earth to be due to the larger auto-correlation of soil moisture.

Combining the results of sections 3.1 and 3.2 we conclude that spring soil moisture deficit in Southern Europe and the phase of the AMV are two slow drivers of similar importance for heat waves in Europe. However, they produce different patterns of positive and negative influence. We note that EC-Earth presents a different result, with a much stronger influence of spring soil moisture, but we don't have enough evidence to conclude that this model is biased.

We also tried to investigate the mechanisms by which the AMV influence the frequency and intensity of heat waves over Europe. To this aim, we plotted the mean response maps to the AMV phase for cloud cover, latent heat, sensible heat, 500hPa geopotential height, precipitation, and soil moisture averaged over the June, July and August period (fig. 10 in appendix A). There is no significance in the responses for individual models. Moreover, the responses are inconsistent between different models. This prevents the interpretation of these maps.

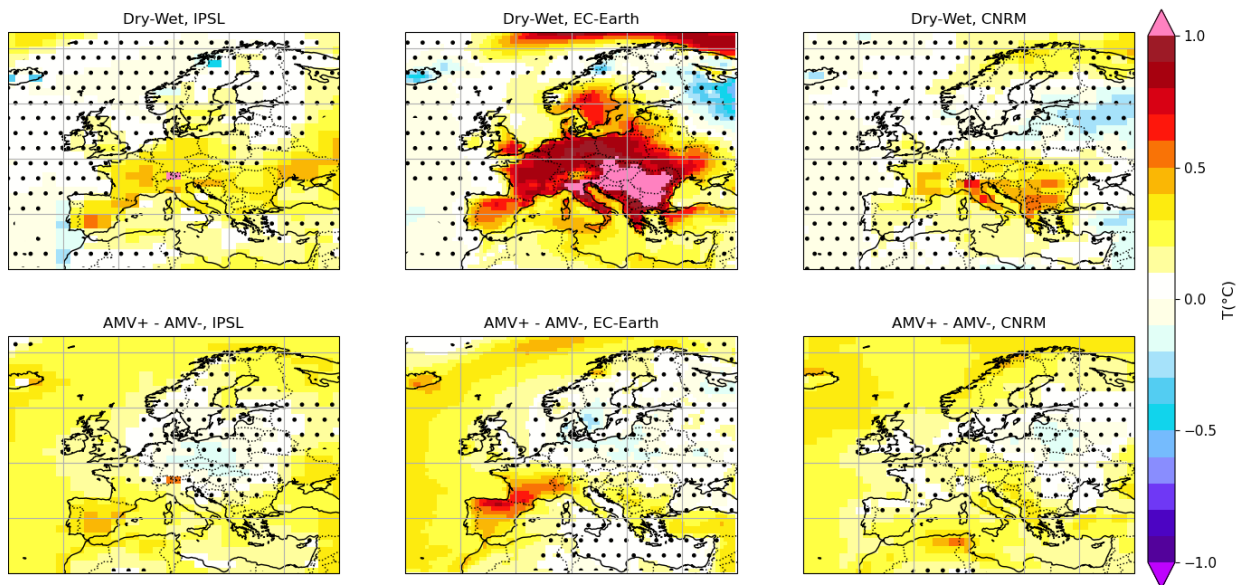


Figure 4: *Mean response maps for 14-day heat waves.* Difference in the mean value of \tilde{A} (defined in eq. (1)) between (top line) the Dry and the Wet ensembles and (bottom line) the AMV+ and AMV- ensembles for each of the three models. Stippling denotes area below the 95% significance level according to a bootstrap test.

4 Influence of the Atlantic Multidecadal Variability and of soil moisture on heat waves with return times from 10 to 50 years

The heat waves that we considered in the previous section are not really rare events. Indeed, the second definition gives one value of \tilde{A} for each year, while for the first definition the fraction of years

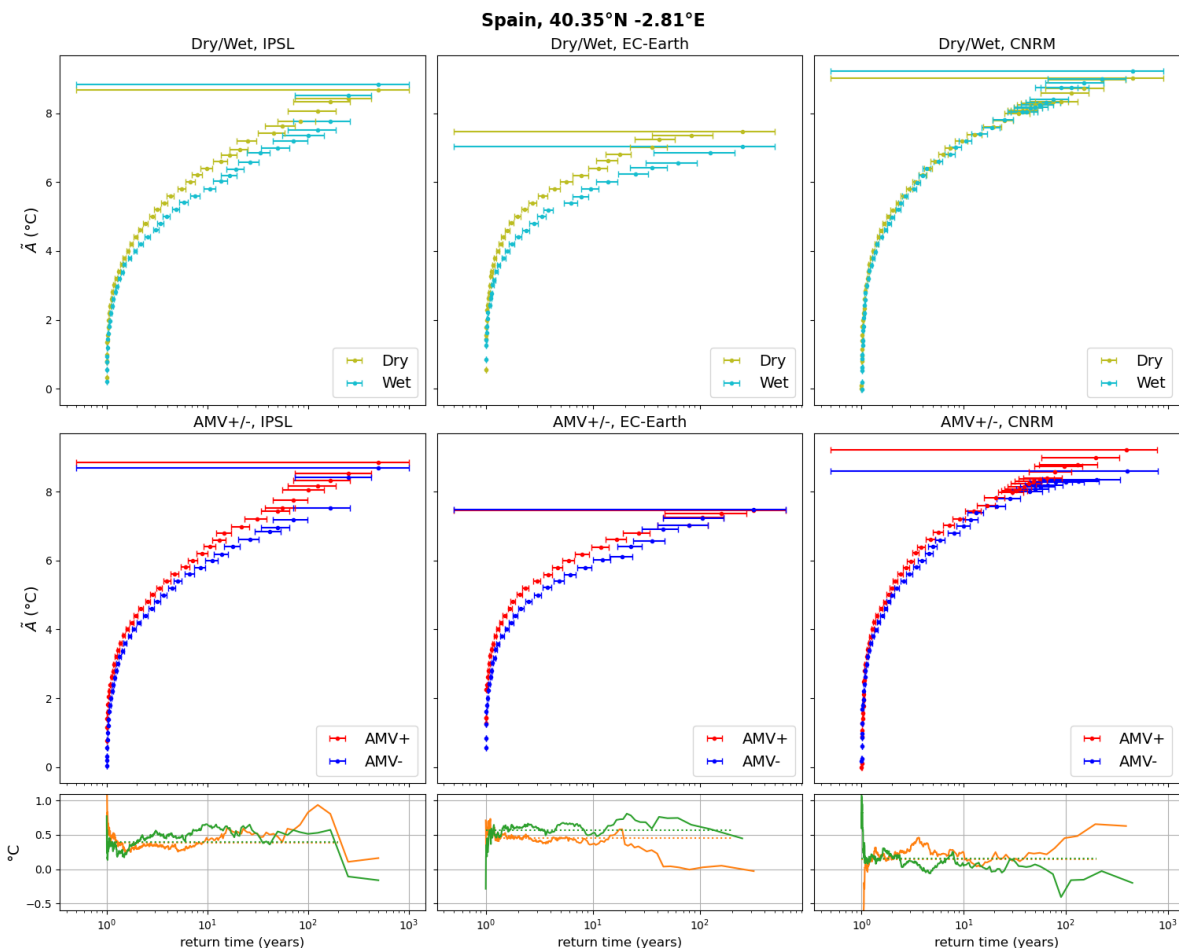


Figure 5: *Return time curves of the intensity of 14-day heat waves.* The two first lines show the temperature anomaly as a function of the return time for the dry and wet ensembles (top row) and the AMV+ and AMV- ensembles (second row) for the three models. Errorbars correspond to one standard deviation of the estimated return time to observe an event of a given amplitude. The third row shows the Dry - Wet (green) and AMV+ - AMV- (orange) differences as a function of the return time. The dotted lines indicate the mean difference values. For each model the chosen grid point covers the coordinate indicated in the figure title which corresponds to a location in the Northeast of Spain, close to the Mediterranean Sea.

during which at least one heat wave occurs is consistently comprised between 50% and 80% for all models and land grid points (not shown). In this section we focus on rarer events with return time of a few decades. In section 4.1 we use return time plots to see how the influence of the slow drivers evolves with the return time for a single grid point. However, this provides information only at a local level. To study extreme events at the European level, we introduce return time maps in section 4.2. Based on these maps, we study extreme events with return times ranging from 10 to 50 years.

4.1 Study of rare events using local return time plots

In climate statistics, the probability of an event is often expressed in terms of return time: if an event has a probability $1/Y$ to occur each year, then it has a return time of Y year, which also corresponds to the average duration between two such events. A classical way to visualize the intensity of events of decreasing probability is to build return time curves: events are ranked by decreasing intensity $a_1 > a_2 > \dots > a_N$ and the empirical return time associated to the level a_m reads:

$$\hat{r}(a_m) = \frac{N}{m}. \quad (2)$$

This is simply the inverse of the empirical probability to have an event of intensity at least as large as a_m which is m/N . By construction, the minimal event's intensity has a return time of one year, the median a return time of two years and the largest event is associated with a return time of N years. In the present study, a will be either the number of heat wave days in a year (following the definition of section 2.3.1) or the 14-day heat wave intensity defined in section 2.3.2. Remember that both quantities are defined at each grid point. We present results for the second definition in this section. The results for the first definition are similar and the corresponding figures are shown in appendix A.

Figure 5 shows the return time curves for the intensity of 14-day heat waves for a grid point in the Northeast of Spain. We chose this region for illustration purposes, as it is one where we observe a strong response of \tilde{A} to both the AMV and the soil moisture in all models, except for the AMV in CNRM (fig. 4). The six upper panels show the empirical return time curves for each ensemble (AMV+, AMV-, Dry, Wet) and each model³. Several considerations arise from these plots. The temperature anomaly starts at about 0°C for a return time close to 1 year⁴, goes up quickly to around 4 or 5°C for a return time of 2 years and then rises at a slower pace, up to anomalies of 7°C to 9°C, depending on the model, for return times of a few centuries. More importantly, these curves allow to visualize how the influence of the drivers on the frequency of events changes as the return level increases. For temperature anomalies from 4°C to 6°C a low soil moisture (resp. a positive AMV phase) double the frequency of occurrence with respect to a high soil moisture (resp. a negative AMV phase) in IPSL and EC-Earth. In CNRM the AMV response is smaller and there is no visible influence of soil moisture.

It is less straightforward to visualize the changes in the influence of the drivers on the intensity of the events. At a first glance, it seems that the influence on the intensity increases with the return time. However, this interpretation is misleading, as it is influenced by the near-vertical alignment of the curves for the lowest return times. Indeed, if two curves are concave and a constant vertical distance away, then the horizontal distance between them grows along the x-*abscissa*⁵. To properly visualize the evolution of the influence of the drivers as the return time increases, we show the Dry - Wet and AMV+ - AMV- differences as a function of the return time on the third line of fig. 5. We see that the influence of both the AMV and soil moisture is roughly constant from a return time of less than two years up to a few decades. There are large fluctuations at very short and large return times which correspond to the two tails of the distribution. The influences of the AMV and soil moisture are of the same order within each model. However, they are lower in CNRM than in the two other models. Figure 11 shows similar return time plots for the threshold based definition.

While return time plots give a view of the evolution of extreme events intensity when shifting from small to large return times, the information they provide is location dependent. For instance, while EC-Earth produces noticeably lower extreme heat waves than the other two models at the location examined in fig. 5, it turns out to be the opposite in Central Europe (not shown). We present in the next section a method to overcome this limitation and obtain a global picture of the influence of the drivers on extreme events.

4.2 Global picture of the influence of the drivers on heat waves with return times of 10 and 50 years

In order to synthesize at the continental scale the local results described above, we introduce the *return time maps*.

Method For each grid point, we consider the difference between AMV+ and AMV- or Dry and Wet return time curves averaged over all the events with return time larger than a threshold RT. This amounts to average the difference between the two curves over the rightmost points in each panel of fig. 5. We considered thresholds values RT=10 and 50 years, which provide a compromise between studying extreme events and keeping enough events to calculate statistics.

³The curve for the dry/wet ensembles on one side and for the AMV+/- ensembles on the other side are very similar for each model because they are built from the same dataset.

⁴Very few events have an anomaly between -2°C and 0°C. They correspond to extreme cold years. They have been cropped for the sake of plot's readability.

⁵As a simple example, one can consider the two curves $y_1(x) = \sqrt{x}$ and $y_2(x) = y_1(x) + \Delta y$. The horizontal distance between them is $\Delta x = 2\Delta y\sqrt{x} - \Delta y^2$ which grows as \sqrt{x} .

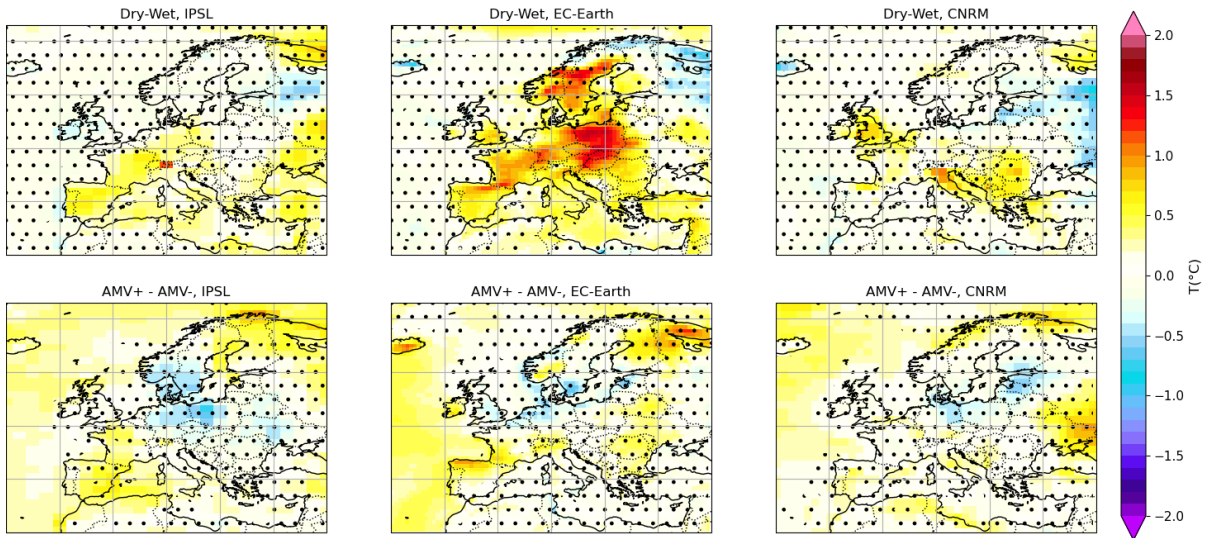


Figure 6: *10 years return time maps for 14-day heat waves.* The maps show the difference of \tilde{A} between (top line) the Dry and Wet ensembles and (bottom line) the AMV+ and AMV- ensembles, conditioned over events with return time greater than 10 years. Stippling denotes area below the 95% significance level according to a bootstrap test.

To be more specific, for each dataset $\mathcal{S} \in \{\text{AMV+}, \text{AMV-}, \text{Dry}, \text{Wet}\}$ and for the return times $\text{RT}=10$ or 50 years, we compute at each grid point:

$$a_{\text{RT}}^{\mathcal{S}}(\mathbf{r}) = \frac{1}{K} \sum_{i=1}^K a_i(\mathbf{r}) \quad \text{where } K = \frac{N_{\mathcal{S}}}{\text{RT}} \quad (3)$$

where \mathbf{r} is the spatial coordinate, $N_{\mathcal{S}}$ is the number of years available in the dataset \mathcal{S} and K is the number of years such that $\hat{r}(a_i) \geq \text{RT}$. We recall that the a_i 's are the number of heat wave days in a year or 14-day heat wave intensity, depending on the definition considered. We have assumed that $a_1 > a_2 > a_3 > \dots > a_{N_{\mathcal{S}}}$ in each dataset. The interpretation is that $a_{10\text{yrs}}^{\mathcal{S}}$ is the empirical mean of 10-year events in the dataset \mathcal{S} . We then display for each grid point the differences $a_{\text{RT}}^{\text{AMV+}}(\mathbf{r}) - a_{\text{RT}}^{\text{AMV-}}(\mathbf{r})$ and $a_{\text{RT}}^{\text{Dry}}(\mathbf{r}) - a_{\text{RT}}^{\text{Wet}}(\mathbf{r})$. We call these maps *return time maps*.

Figure 6 shows the 10-year return time maps for the intensity of 14-day heat waves. We observe the same global response pattern as for the mean response (see fig. 4) with a positive influence of a positive AMV phase or low soil moisture over most parts of Europe and a negative influence in the Northeast. The regions of negative influence have extended in size and are located in Russia for the soil moisture and around the Baltic sea for the AMV. In many areas, the 10-year response is higher than the mean response with an amplitude up to 1°C. Once again, EC-Earth shows a higher response to soil moisture with a peak amplitude of 1.8°C. We note that the peak of this response has shifted northward with respect to the mean response. Each individual map shows only reduced area of statistical significance. This is because we compute averages over only one tenth of our available years. However, we note that the global response pattern is consistent among all three models, which gives confidence in the significance of the signal.

We now focus on more extreme events and present the 50-year return time maps of 14-day heat waves intensity on fig. 7. We can distinguish the same global patterns as on fig. 6. The regions of negative influence have again extended in size and new ones have appeared. The amplitude of the response is higher than for 10-year events and goes up to 2°C in some locations. However, the bottom line of fig. 5 shows that there are large fluctuations of the response for events of return time larger

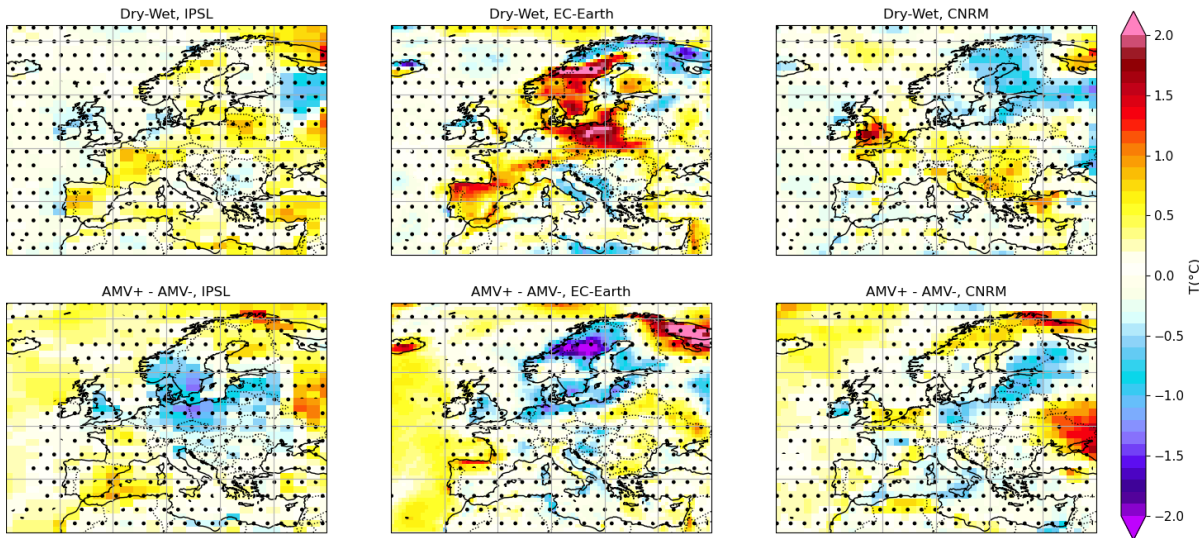


Figure 7: 50 years return time maps for 14-day heat waves. The maps show the difference of $\tilde{\Delta}$ between (top line) the Dry and Wet ensembles and (bottom line) the AMV+ and AMV- ensembles, conditioned over events with return time greater than 50 years. Stippling denotes area below the 95% significance level according to a bootstrap test.

than a few decades because we are in the very tail of the empirical distribution. Here we do not have enough data to discriminate if these regions of high response are real impacts of the AMV and soil moisture or if they are only due to large fluctuations in the tail of the distribution.

We performed the same analysis for the number of heat wave days per year as measured by the threshold-based definition. The 10 and 50-year return time maps for this definition are shown on figs. 12 and 13 in appendix A. The global response patterns are similar to the ones for the intensity of 14-day heat waves, leading to the same conclusions.

5 Conclusion

In this study, we use data from the DCPD coupled model intercomparison project to assess which slow driver, between the AMV and spring soil moisture in Southern Europe, has the most influence on European heat waves. We compare the influence of the drivers being both one standard deviation higher or lower than the climatology. We use two complementary definitions of heat waves and we focus on typical and extreme events across Europe.

In order to decouple the effects of the two drivers, we first investigated the influence of the AMV over the distribution of spring soil moisture averaged over Southern Europe, (right panel of fig. 1). We found that it was negligible in two models (IPSL and CNRM) while there is a small but significant influence in EC-Earth where the average soil moisture is 10.5 kg.m^{-2} lower in the AMV+ phase compared to the AMV- phase. This can be compared to the standard deviation computed over the two ensembles together which is $\sigma_{\text{EC-Earth}}^{\text{SM}} = 34.4 \text{ kg.m}^{-2}$. We conclude that the two drivers can be studied independently in IPSL and CNRM. For EC-Earth, there is an indirect influence on the AMV on heat waves through a decreased soil moisture in the positive AMV phase.

Heat waves - in both definitions - show similar responses to the influence of the AMV and soil moisture. In two models (IPSL and CNRM), we found that the influence of a one sigma forcing of either driver is of comparable amplitude and pattern. In EC-Earth the soil moisture has a greater influence, with a higher response over a large area in Central Europe, as shown by fig. 4. This can be linked to the higher persistence of this variable along the summer season, as shown in fig. 3. Coherently to previous studies [17], a positive AMV phase or low soil moisture induce more heat wave days and

hotter heat waves over most of Europe. However, there are also regions of negative influence which are located in the North-East of Europe with responses down to -0.2°C for the mean temperature of 14-day heat waves (fig. 4) and 1 less heat wave day per year (fig. 2). This cold response is located over Russia for the soil moisture and over Central Europe for the AMV. We hypothesize that, besides a direct heating effect in phase with the main surface temperature forcing, the dynamical atmospheric response creates a cold area downstream. This would explain why the cold area linked to the soil moisture is located eastward of the AMV one. Soil moisture has a largest influence over Southern Europe, up to 50°N , while the AMV influences mainly the Mediterranean basin. The response goes up to 4 more heat wave days per year and $+0.5^{\circ}\text{C}$ for the mean intensity of 14-day heat waves, except for EC-Earth which presents a much larger response to the influence of low soil moisture.

By introducing return time maps, we were able to study extreme heat waves with return times from 10 to 50 years. One main issue in the study of such rare events is the scarcity of data, which causes large area to be below the statistical significance level in fig. 6 and fig. 7. Nevertheless the consistency of the response patterns among the three models suggests the presence of a real signal.

For events with return times of 10 or 50 years, the influences of the AMV and soil moisture increase, according to rather similar regional patterns as for typical events, and remain of similar amplitude. However, the regions where a positive AMV phase or low spring soil moisture induce less heat wave days and cooler heat waves extend. This conclusion is valid for both definitions of heat waves. Positive AMV phases or spring soil moisture deficit induce a 1°C (resp. 2°C) increase of the temperature for heat waves with 10-year (resp. 50-year) return times. They also increase the number of heat wave days by to 9 days/year (resp. 13 days/year) for heat waves with 10-year (resp. 50-year) return times. Once again, the influence of spring soil moisture on these extreme events is greater in EC-Earth than in the other two models.

Our study points out a discrepancy in the response to soil moisture anomalies between EC-Earth and IPSL and CNRM models. Our analysis of the auto-correlation of soil moisture shows that this variable has a stronger memory in EC-Earth and it might be due to its land model. However, we could not discriminate with confidence if one model was more biased than the others. Further investigations need to be done in this and other models to gain a more confident understanding of the response of heat waves to spring soil moisture anomalies.

We now discuss our work in the context of climate change and draw some perspectives. We showed that the AMV can modulate the amplitude of 14-day European heat waves by 0.5°C to 1°C . This can be put in perspective with the current warming rate of hot extremes in Europe. Vautard et al. [44] showed that the warming rate of hot extremes (TXx) over Europe is comprised between 2°C and 6°C per global warming degree with the fastest warming being over Western Europe. The current global warming rate being about 0.2°C per decade, this corresponds to a warming of 0.4°C to 1.2°C per decades for hot extremes, which is of the same order of magnitude as the modulation by the AMV. This means that the phase of the AMV can either mask or exacerbate the warming trend of hot extremes.

A similar conclusion was already discussed in ref. [45] for the seasonal averaged temperature: the internal variability, including the AMV, will modulate the global warming trend at the European scale, either mitigating or exacerbating its effects. Moreover, these authors argued that, in the near term, the internal variability of the climate system will have a stronger influence on the European averaged temperature than the SSP emission scenario that we will actually follow. It is a natural question to ask whether this might be true also for the case of extreme heat waves, as studied in this paper. This is however beyond the scope of our article, as it would require a specific study of the impact of the different scenario on extreme event statistics. We leave this question as an interesting perspective for future works.

In a warming climate, the Mediterranean basin is projected to become dryer [3]. This suggests that, when considering the effect of climate change, the variability of the soil moisture over the zone considered for this study might be reduced, leading to a reduced importance in the modulation of heat waves. However, the transition zone between dry and wet climate, in which the variability of soil moisture is large, is expected to shift northward with respect to the Mediterranean basin. Thus it could be relevant to look for the region of largest soil moisture variability in the future and to consider the soil moisture in this region as the relevant slow driver for European heat waves. Such a prospective study would be a natural follow-up to this work.

A clear limitation of this study comes from the scarcity of data one would rapidly face if one would wish to study events with higher return times, for instance a century. As we mentioned before, we

are already crossing this regime of lack of data with return times of a decade. Recently, rare event algorithms have been designed to enhance the sampling of extreme events in numerical simulations at low computation cost. This class of algorithms have been recently applied successfully to sample heat waves with return times of a century or even tens of millennia in some regions of Europe [38, 40] and South Asia [46]. Using such rare event algorithm could be a promising path to study the influence of slow drivers on heat waves with return times of a century or more.

Acknowledgements

The authors thank the modelling groups who took part in the DCP-C AMV experiment. The model data were accessed through the IPSL mesocenter ESPRI facility which is supported by CNRS, UPMC, Labex L-IPSL, CNES and Ecole Polytechnique. We also thank the Centre Blaise Pascal of the Ecole Normale Supérieure de Lyon for the computation resources used to carry on the study and Emmanuel Quemener for his help with the platform. We are grateful to C. Ardilouze for suggesting to plot the soil moisture auto-correlation and bringing GLEAM dataset to our attention. We thank C. Cassou, S. Qasmi and H. Douville for enlightening discussions.

Conflict of Interest

The authors declare no conflicts of interests.

Study fundings

V.M. is part of the EDIPI ITN, which has received funding from the European Union's Horizon 2020 research and innovation program under the Marie Skłodowska-Curie grant agreement No 956396. C.L.P. is funded by the ANR grant SAMPRACE, Project No. ANR-20-CE01-0008-01.

Author Contributions

F.B. and F.D.A. proposed the project and provided guidance for the research. V.M. and C.L.P. conducted the research, performed all analysis and wrote the first draft of the manuscript. All authors contributed to manuscript review and editing.

Data Availability

All data used in this article are publicly available. Model simulation results can be accessed via the ESGF grid, for instance at <https://esgf-node.ipsl.upmc.fr/search/cmip6-ipsl/>. ERA5-Land monthly dataset, was downloaded from Copernicus Climate Data Store: <https://cds.climate.copernicus.eu>. The GLEAM evaporation dataset can be downloaded from <https://www.gleam.eu/>. The processed data used in this research will be shared on reasonable request to the corresponding author.

References

- [1] James Hansen, Makiko Sato, and Reto Ruedy. Perception of climate change. *Proceedings of the National Academy of Sciences*, 109(37):E2415–E2423, September 2012. Publisher: Proceedings of the National Academy of Sciences.
- [2] Hans-Otto Pörtner, Debra C. Roberts, Melinda M. B. Tignor, Elvira Poloczanska, Katja Mintenbeck, Andrés Alegría, Marlies Craig, Stefanie Langsdorf, Sina Löschke, Vincent Möller, Andrew Okem, and Bardhyl Rama. IPCC 2022: Climate Change 2022 : Impacts, adaptation and vulnerability : Working group II contribution to the sixth assessment report of the intergovernmental panel on climate change. Report, Cambridge University Press, Cambridge, UK, 2022.

- [3] Intergovernmental Panel On Climate Change. *Climate Change 2021 – The Physical Science Basis: Working Group I Contribution to the Sixth Assessment Report of the Intergovernmental Panel on Climate Change*. Cambridge University Press, 1 edition, July 2023.
- [4] Efi Rousi, Kai Kornhuber, Goratz Beobide-Arsuaga, Fei Luo, and Dim Coumou. Accelerated western European heatwave trends linked to more-persistent double jets over Eurasia. *Nature Communications*, 13(1):3851, July 2022. Publisher: Nature Publishing Group.
- [5] Sarah E. Perkins. A review on the scientific understanding of heatwaves—Their measurement, driving mechanisms, and changes at the global scale. *Atmospheric Research*, 164-165:242–267, October 2015.
- [6] Radley M. Horton, Justin S. Mankin, Corey Lesk, Ethan Coffel, and Colin Raymond. A Review of Recent Advances in Research on Extreme Heat Events. *Current Climate Change Reports*, 2(4):242–259, December 2016.
- [7] Randall Dole, Martin Hoerling, Judith Perlwitz, Jon Eischeid, Philip Pegion, Tao Zhang, Xiao-Wei Quan, Taiyi Xu, and Donald Murray. Was there a basis for anticipating the 2010 Russian heat wave? *Geophysical Research Letters*, 38(6), 2011. _eprint: <https://onlinelibrary.wiley.com/doi/pdf/10.1029/2010GL046582>.
- [8] Siegfried Schubert, Hailan Wang, and Max Suarez. Warm Season Subseasonal Variability and Climate Extremes in the Northern Hemisphere: The Role of Stationary Rossby Waves. *Journal of Climate*, 24(18):4773–4792, September 2011. Publisher: American Meteorological Society Section: Journal of Climate.
- [9] R. Vautard, P. Yiou, F. D’Andrea, N. de Noblet, N. Viovy, C. Cassou, J. Polcher, P. Ciais, M. Kageyama, and Y. Fan. Summertime European heat and drought waves induced by wintertime Mediterranean rainfall deficit. *Geophysical Research Letters*, 34(7):L07711, April 2007.
- [10] Matteo Zampieri, Fabio D’Andrea, Robert Vautard, Philippe Ciais, Nathalie De Noblet-Ducoudré, and Pascal Yiou. Hot European Summers and the Role of Soil Moisture in the Propagation of Mediterranean Drought. *Journal of Climate*, 22(18):4747–4758, September 2009.
- [11] E. M. Fischer, S. I. Seneviratne, D. Lüthi, and C. Schär. Contribution of land-atmosphere coupling to recent European summer heat waves. *Geophysical Research Letters*, 34(6):L06707, March 2007.
- [12] E. M. Fischer, S. I. Seneviratne, P. L. Vidale, D. Lüthi, and C. Schär. Soil Moisture–Atmosphere Interactions during the 2003 European Summer Heat Wave. *Journal of Climate*, 20(20):5081–5099, October 2007.
- [13] Lisa Alexander. Extreme heat rooted in dry soils. *Nature Geoscience*, 4(1):12–13, January 2011. Number: 1 Publisher: Nature Publishing Group.
- [14] Stefano Materia, Constantin Ardilouze, Chloé Prodhomme, Markus G. Donat, Marianna Benassi, Francisco J. Doblas-Reyes, Daniele Peano, Louis-Philippe Caron, Paolo Ruggieri, and Silvio Gualdi. Summer temperature response to extreme soil water conditions in the Mediterranean transitional climate regime. *Climate Dynamics*, 58(7):1943–1963, April 2022.
- [15] Rowan T. Sutton and Buwen Dong. Atlantic Ocean influence on a shift in European climate in the 1990s. *Nature Geoscience*, 5(11):788–792, November 2012.
- [16] Saïd Qasmi, Christophe Cassou, and Julien Boé. Teleconnection Between Atlantic Multidecadal Variability and European Temperature: Diversity and Evaluation of the Coupled Model Intercomparison Project Phase 5 Models. *Geophysical Research Letters*, 44(21):11,140–11,149, 2017. _eprint: <https://onlinelibrary.wiley.com/doi/pdf/10.1002/2017GL074886>.
- [17] Saïd Qasmi, Emilia Sanchez-Gomez, Yohan Ruprich-Robert, Julien Boé, and Christophe Cassou. Modulation of the Occurrence of Heatwaves over the Euro-Mediterranean Region by the Intensity of the Atlantic Multidecadal Variability. *Journal of Climate*, 34(3):1099–1114, February 2021.

- [18] Rowan T. Sutton and Daniel L. R. Hodson. Atlantic Ocean Forcing of North American and European Summer Climate. *Science*, 309(5731):115–118, July 2005. Publisher: American Association for the Advancement of Science.
- [19] Yohan Ruprich-Robert, Rym Msadek, Frederic Castruccio, Stephen Yeager, Tom Delworth, and Gokhan Danabasoglu. Assessing the Climate Impacts of the Observed Atlantic Multidecadal Variability Using the GFDL CM2.1 and NCAR CESM1 Global Coupled Models. *Journal of Climate*, 30(8):2785–2810, April 2017.
- [20] Yohan Ruprich-Robert, Thomas Delworth, Rym Msadek, Frederic Castruccio, Stephen Yeager, and Gokhan Danabasoglu. Impacts of the Atlantic Multidecadal Variability on North American Summer Climate and Heat Waves. *Journal of Climate*, 31(9):3679–3700, May 2018.
- [21] Jeff R. Knight, Robert J. Allan, Chris K. Folland, Michael Vellinga, and Michael E. Mann. A signature of persistent natural thermohaline circulation cycles in observed climate. *Geophysical Research Letters*, 32(20), 2005. eprint: <https://onlinelibrary.wiley.com/doi/pdf/10.1029/2005GL024233>.
- [22] S. G. Yeager and J. I. Robson. Recent Progress in Understanding and Predicting Atlantic Decadal Climate Variability. *Current Climate Change Reports*, 3(2):112–127, June 2017.
- [23] Christophe Cassou, Yochanan Kushnir, Ed Hawkins, Anna Pirani, Fred Kucharski, In-Sik Kang, and Nico Caltabiano. Decadal Climate Variability and Predictability: Challenges and Opportunities. *Bulletin of the American Meteorological Society*, 99(3):479–490, March 2018.
- [24] James W. Hurrell and Clara Deser. North Atlantic climate variability: The role of the North Atlantic Oscillation. *Journal of Marine Systems*, 79(3):231–244, February 2010.
- [25] Thomas L. Delworth, Fanrong Zeng, Gabriel A. Vecchi, Xiaosong Yang, Liping Zhang, and Rong Zhang. The North Atlantic Oscillation as a driver of rapid climate change in the Northern Hemisphere. *Nature Geoscience*, 9(7):509–512, July 2016. Number: 7 Publisher: Nature Publishing Group.
- [26] Jean-Marie Robine, Siu Lan K. Cheung, Sophie Le Roy, Herman Van Oyen, Clare Griffiths, Jean-Pierre Michel, and François Richard Herrmann. Death toll exceeded 70,000 in Europe during the summer of 2003. *Comptes Rendus Biologies*, 331(2):171–178, 2008.
- [27] Ngar-Cheung Lau and Mary Jo Nath. A Model Study of Heat Waves over North America: Meteorological Aspects and Projections for the Twenty-First Century. *Journal of Climate*, 25(14):4761–4784, July 2012.
- [28] George J. Boer, Douglas M. Smith, Christophe Cassou, Francisco Doblas-Reyes, Gokhan Danabasoglu, Ben Kirtman, Yochanan Kushnir, Masahide Kimoto, Gerald A. Meehl, Rym Msadek, Wolfgang A. Mueller, Karl E. Taylor, Francis Zwiers, Michel Rixen, Yohan Ruprich-Robert, and Rosie Eade. The Decadal Climate Prediction Project (DCPP) contribution to CMIP6. *Geoscientific Model Development*, 9(10):3751–3777, October 2016.
- [29] Olivier Boucher, Jérôme Servonnat, Anna Lea Albright, Olivier Aumont, Yves Balkanski, Vladislav Bastrikov, Slimane Bekki, Rémy Bonnet, Sandrine Bony, Laurent Bopp, Pascale Braconnot, Patrick Brockmann, Patricia Cadule, Arnaud Caubel, Frederique Cheruy, Francis Codron, Anne Cozic, David Cugnet, Fabio D’Andrea, Paolo Davini, Casimir Lavergne, Sébastien Denvil, Julie Deshayes, Marion Devilliers, Agnes Ducharne, Jean-Louis Dufresne, Elliott Dupont, Christian Éthé, Laurent Fairhead, Lola Falletti, Simona Flavoni, Marie-Alice Foujols, Sébastien Gardoll, Guillaume Gastineau, Josefine Ghattas, Jean-Yves Grandpeix, Bertrand Guenet, Lionel Guez, E., Eric Guilyardi, Matthieu Guimberteau, Didier Hauglustaine, Frédéric Hourdin, Abderrahmane Idelkadi, Sylvie Joussaume, Masa Kageyama, Myriam Khodri, Gerhard Krinner, Nicolas Lebas, Guillaume Levassieur, Claire Lévy, Laurent Li, François Lott, Thibaut Lurton, Sebastiaan Luyssaert, Gurvan Madec, Jean-Baptiste Madeleine, Fabienne Maignan, Marion Marchand, Olivier Marti, Lidia Mellul, Yann Meurdesoif, Juliette Mignot, Ionela Musat, Catherine Ottlé, Philippe Peylin, Yann Planton, Jan Polcher, Catherine Rio, Nicolas Rochetin, Clément Rousset,

- Pierre Sepulchre, Adriana Sima, Didier Swingedouw, Rémi Thiéblemont, Abdoul Khadre Traore, Martin Vancoppenolle, Jessica Vial, Jérôme Vialard, Nicolas Viovy, and Nicolas Vuichard. Presentation and Evaluation of the IPSL-CM6A-LR Climate Model. *Journal of Advances in Modeling Earth Systems*, 12(7), July 2020.
- [30] Ralf Döscher, Mario Acosta, Andrea Alessandri, Peter Anthoni, Almut Arneth, Thomas Arsouze, Tommi Bergmann, Raffaele Bernadello, Souhail Boussetta, Louis-Philippe Caron, Glenn Carver, Miguel Castrillo, Franco Catalano, Ivana Cvijanovic, Paolo Davini, Evelien Dekker, Francisco J. Doblas-Reyes, David Docquier, Pablo Echevarria, Uwe Fladrich, Ramon Fuentes-Franco, Matthias Gröger, Jost v. Hardenberg, Jenny Hieronymus, M. Pasha Karami, Jukka-Pekka Keskinen, Torben Koenigk, Risto Makkonen, Francois Massonnet, Martin Ménégoz, Paul A. Miller, Eduardo Moreno-Chamarro, Lars Nieradzic, Twan van Noije, Paul Nolan, Declan O'Donnell, Pirkka Olinaho, Gijs van den Oord, Pablo Ortega, Oriol Tintó Prims, Arthur Ramos, Thomas Reerink, Clement Rousset, Yohan Ruprich-Robert, Philippe Le Sager, Torben Schmith, Roland Schrödner, Federico Serva, Valentina Sicardi, Marianne Sloth Madsen, Benjamin Smith, Tian Tian, Etienne Tourigny, Petteri Uotila, Martin Vancoppenolle, Shiyu Wang, David Wärlind, Ulrika Willén, Klaus Wyser, Shuting Yang, Xavier Yepes-Arbós, and Qiong Zhang. The EC-Earth3 Earth System Model for the Climate ModelIntercomparison Project 6. preprint, Climate and Earth system modeling, February 2021.
- [31] A. Voldoire, D. Saint-Martin, S. Sénési, B. Decharme, A. Alias, M. Chevallier, J. Colin, J.-F. Guérémy, M. Michou, M.-P. Moine, P. Nabat, R. Roehrig, D. Salas y Méliá, R. Sférian, S. Valcke, I. Beau, S. Belamari, S. Berthet, C. Cassou, J. Cattiaux, J. Deshayes, H. Douville, C. Ethé, L. Franchistéguy, O. Geoffroy, C. Lévy, G. Madec, Y. Meurdesoif, R. Msadek, A. Ribes, E. Sanchez-Gomez, L. Terray, and R. Waldman. Evaluation of CMIP6 DECK Experiments With CNRM-CM6-1. *Journal of Advances in Modeling Earth Systems*, 11(7):2177–2213, July 2019.
- [32] Joaquín Muñoz-Sabater, Emanuel Dutra, Anna Agustí-Panareda, Clément Albergel, Gabriele Arduini, Gianpaolo Balsamo, Souhail Boussetta, Margarita Choulga, Shaun Harrigan, Hans Hersbach, Brecht Martens, Diego G. Miralles, María Piles, Nemesio J. Rodríguez-Fernández, Ervin Zsoter, Carlo Buontempo, and Jean-Noël Thépaut. ERA5-Land: a state-of-the-art global reanalysis dataset for land applications. *Earth System Science Data*, 13(9):4349–4383, September 2021. Publisher: Copernicus GmbH.
- [33] D. G. Miralles, T. R. H. Holmes, R. a. M. De Jeu, J. H. Gash, A. G. C. A. Meesters, and A. J. Dolman. Global land-surface evaporation estimated from satellite-based observations. *Hydrology and Earth System Sciences*, 15(2):453–469, February 2011. Publisher: Copernicus GmbH.
- [34] Brecht Martens, Diego G. Miralles, Hans Lievens, Robin van der Schalie, Richard A. M. de Jeu, Diego Fernández-Prieto, Hylke E. Beck, Wouter A. Dorigo, and Niko E. C. Verhoest. GLEAM v3: satellite-based land evaporation and root-zone soil moisture. *Geoscientific Model Development*, 10(5):1903–1925, May 2017. Publisher: Copernicus GmbH.
- [35] Christoph Schär, Pier Luigi Vidale, Daniel Lüthi, Christoph Frei, Christian Häberli, Mark A. Liniger, and Christof Appenzeller. The role of increasing temperature variability in European summer heatwaves. *Nature*, 427(6972):332–336, January 2004. Publisher: Nature Publishing Group.
- [36] David Barriopedro, Erich M. Fischer, Jürg Luterbacher, Ricardo M. Trigo, and Ricardo García-Herrera. The Hot Summer of 2010: Redrawing the Temperature Record Map of Europe. *Science*, 332(6026):220–224, April 2011. Publisher: American Association for the Advancement of Science.
- [37] Dim Coumou and Stefan Rahmstorf. A decade of weather extremes. *Nature Climate Change*, 2(7):491–496, July 2012. Publisher: Nature Publishing Group.
- [38] Francesco Ragone, Jeroen Wouters, and Freddy Bouchet. Computation of extreme heat waves in climate models using a large deviation algorithm. *Proceedings of the National Academy of Sciences*, 115(1):24–29, January 2018.

-
- [39] Francesco Ragone and Freddy Bouchet. Computation of Extreme Values of Time Averaged Observables in Climate Models with Large Deviation Techniques. *Journal of Statistical Physics*, 179(5-6):1637–1665, June 2020.
- [40] F. Ragone and F. Bouchet. Rare Event Algorithm Study of Extreme Warm Summers and Heatwaves Over Europe. *Geophysical Research Letters*, 48(12):e2020GL091197, June 2021.
- [41] Vera Melinda Gálfi, Valerio Lucarini, and Jeroen Wouters. A large deviation theory-based analysis of heat waves and cold spells in a simplified model of the general circulation of the atmosphere. *Journal of Statistical Mechanics: Theory and Experiment*, 2019(3):033404, March 2019. Publisher: IOP Publishing and SISSA.
- [42] Vera Melinda Galfi and Valerio Lucarini. Fingerprinting Heatwaves and Cold Spells and Assessing Their Response to Climate Change Using Large Deviation Theory. *Physical Review Letters*, 127(5):058701, July 2021. Publisher: American Physical Society.
- [43] Vera Melinda Gálfi, Valerio Lucarini, Francesco Ragone, and Jeroen Wouters. Applications of large deviation theory in geophysical fluid dynamics and climate science. *La Rivista del Nuovo Cimento*, 44(6):291–363, June 2021.
- [44] Robert Vautard, Julien Cattiaux, Tamara Happé, Jitendra Singh, Rémy Bonnet, Christophe Cassou, Dim Coumou, Fabio D’Andrea, Davide Faranda, Erich Fischer, Aurélien Ribes, Sebastian Sippel, and Pascal Yiou. Heat extremes in Western Europe increasing faster than simulated due to atmospheric circulation trends. *Nature Communications*, 14(1):6803, October 2023. Publisher: Nature Publishing Group.
- [45] Aurélien Liné, Christophe Cassou, Rym Msadek, and Parey Parey. Assessment of climate change at near-term (2020-2040) over northern europe through internal variability storylines. *submitted to NPJ*, 2023.
- [46] Clément Le Priol, Joy M. Monteiro, and Freddy Bouchet. Using rare event algorithms to understand the statistics and dynamics of extreme heatwave seasons in south asia. *submitted to Environmental Research: Climate*, March 2024.

A Supplementary material

A.1 Methods

Brief descriptions of the models characteristics

- *IPSL* is composed of the LMDZ atmospheric model version 6A-LR, based on a rectangular grid with 144 longitude x 143 latitude equally spaced points, resulting in a resolution of $2.5^\circ \times 1.3^\circ$. It has 79 vertical levels and extends up to 80 km. The ocean component is the NEMO oceanic model version 3.6, with 71 vertical layers and an horizontal resolution of 1° . The land surface model is the ORCHIDEE version 2.0, with 11 layers for a total of 2 m of soil depth. Further information and details can be found at [29].
- *EC-Earth* is composed of the Integrated Forecast System (IFS) CY36R4 of the European Centre for Medium Range Weather Forecasts (ECMWF) atmospheric model, based on a linearly reduced Gaussian grid equivalent to 512 longitude x 256 latitude points with 91 vertical levels. It includes the land-surface scheme HTESSEL. The ocean and sea-ice model is NEMO-LIM3 version 3.6, with 75 vertical layers. Further information and details can be found at [30].
- *CNRM* is composed of the ARPEGE-Climat atmospheric model, version 6.3 with 91 vertical levels. The ocean component is based on the NEMO version 3.6, while the sea ice component is based on GELATO, version 6. Further information and details can be found at [31].

Creation of the Dry and Wet ensembles The Dry and Wet ensembles are made of years coming from the AMV+/- and CTRL ensembles according to SM_{av} . When building the Dry and Wet ensembles we want to make sure that there is no indirect influence of the AMV on the soil moisture through influence of the AMV on SM_{av} . Figure 1 (right) shows the distribution of SM_{av} for each ensemble in the three models. We see that in IPSL and CNRM the phase of the AM does not influence the soil moisture, while in EC-Earth, there is a non negligible influence with the average SM_{av} in the AMV-phase being 5.2 kg.m^{-2} than in the AMV+ phase. To make sure that there is no indirect influence of the AMV we choose to enforce to have the exact same numbers of AMV+ and AMV- years in the Dry and Wet ensembles. This choice also allows us to deal with the imbalance of the CNRM ensemble because of missing runs for Soil Moisture data. We have only 380 years of AMV+ and 280 years of AMV-. We will briefly comment on the procedure to create the ensemble. It is sketched in fig. 8. Each original ensemble (AMV+, AMV-, CTRL) is sorted according to SM_{av} . The k driest years of the AMV+ and AMV- ensembles are put in the Dry ensemble which is completed with the n driest years from the CTRL run when available. For this study, the number of years coming from the AMV experiments, namely k, is different from the one coming from the CTRL, namely n. The reason is the different amount of years available for each experiment, which we detail in table 1. More details about the values of SM_{av} for each model can be found in table 2. We choose the ensemble size such that the mean value of SM_{av} in the Dry (resp. Wet) ensemble is nearly one standard deviation below (resp. above) the mean value SM_{av} averaged over the AMV+/- and CTRL ensembles all-together. This makes the comparison with the AMV forcing sensible because the imposed SST pattern corresponds to one standard deviation of the AMV variability.

	IPSL	EC-Earth	CNRM
Dry	443.1 / 442.5	715.2 / 714.3	383.1 / 383.2
Wet	480.2 / 481.0	782.5 / 783.1	404.6 / 405.7

Table 2: Mean value of SM_{av} (in kg.m^{-2}) in the Dry and Wet ensembles for each model. In each case the values are ordered as *realized* / *target* where *realized* is the computed mean in the Dry or Wet ensemble and *target* corresponds to exactly one standard deviation away from the overall mean value.

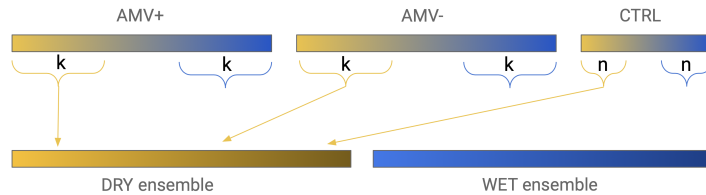


Figure 8: *Sketch of the procedure to create the Dry and Wet ensembles.* Data in each experiments are already sorted according to its SM_{av} value.

Computation of the errorbars on the local RT plots Let A be the random variable of event's amplitudes. Let us fix a return level a . The random variable $X = \mathbf{1}(A \geq a)$ follows a Bernoulli law of parameter $p := \mathbb{P}(A \geq a)$. Let N be the number of years in our dataset and m the number of years where we observe $A \geq a$. Then $\hat{p} = m/N$ is an unbiased estimator of p and we estimate the return time of events larger than a as

$$\hat{r}(a) = \frac{1}{\hat{p}} = \frac{N}{m}. \quad (4)$$

We want to compute an estimate of the error on $\hat{r}(a)$. First, note that the empirical variance of \hat{p} reads $\hat{\sigma}_X^2 = \frac{1}{N-1} \sum_{i=1}^N (X_i - \hat{p})^2 = \frac{N}{N-1} \hat{p}(1 - \hat{p})$.

According to the Central Limit Theorem, the variance of \hat{p} reads $\sigma_{\hat{p}}^2 = \frac{p(1-p)}{N}$ which can be estimated by the empirical formula

$$\hat{\sigma}_{\hat{p}}^2 = \frac{\hat{p}(1 - \hat{p})}{N}.$$

Let us define $\delta = \hat{p} - p$. Note that $\mathbb{E}[\delta] = 0$ and $\sigma_{\delta}^2 = \sigma_{\hat{p}}^2$

Let us assume that in all our observations $\delta < p$ (which is likely to be valid if $\sigma(r) \ll r$). Then we can write:

$$\hat{r} = \frac{1}{\hat{p}} = \frac{1}{p} \times \frac{1}{1 + \delta/p} = \frac{1}{p} \left(1 - \frac{\delta}{p} + \frac{\delta^2}{p^2} + O\left(\frac{\delta^3}{p^3}\right) \right), \quad (5)$$

$$\hat{r}^2 = \frac{1}{n_+^2} = \frac{1}{p^2} \left(1 - \frac{2\delta}{p} + \frac{3\delta^2}{p^2} + O\left(\frac{\delta^3}{p^3}\right) \right). \quad (6)$$

Taking the difference of the expectations we get:

$$\sigma_{\hat{r}}^2 = \mathbb{E}[\hat{r}^2] - \mathbb{E}[\hat{r}]^2 = \frac{\mathbb{E}[\delta^2]}{p^4} + O\left(\frac{\mathbb{E}[\delta^3]}{p^3}\right). \quad (7)$$

The errorbars plotted on the local return time plots figs. 5 and 11 corresponds to the standard deviation of \hat{r} :

$$\sigma_{\hat{r}} \simeq \frac{\sigma(\hat{p})}{p^2} = \frac{1}{p^2} \sqrt{\frac{p(1-p)}{N}} \simeq \hat{r} \sqrt{\frac{\hat{r} - 1}{N}}, \quad (8)$$

where we have used that $1/p = r$.

Note that the domain of validity of this approximation is $\sigma(r) \ll r$ and so these formula is not correct to estimate the error on the most extreme return levels (the ones for which the number of exceedance m is small).

Implementation of the bootstrap test We implemented a bootstrap to test the significance of the AMV+ - AMV- and Dry-Wet differences in all maps. The procedure is the same for each model, but was slightly adapted for CNRM to take into account the fact that the AMV+ and AMV- do not have the same size and that the soil moisture of some members is missing.

Concretely, we pooled the results from all experiments (AMV+/- and CTRL) together to obtain a single large dataset for each model. From this large dataset, we draw $N=1000$ samples of M years, where M is equal to the number of year in each dataset displayed in table 1. For each sample we compute the average over the sample, as well as the 10-year and 50-year return time maps. For each of those maps (average, 10-year and 50-year return time maps), we build the empirical distribution

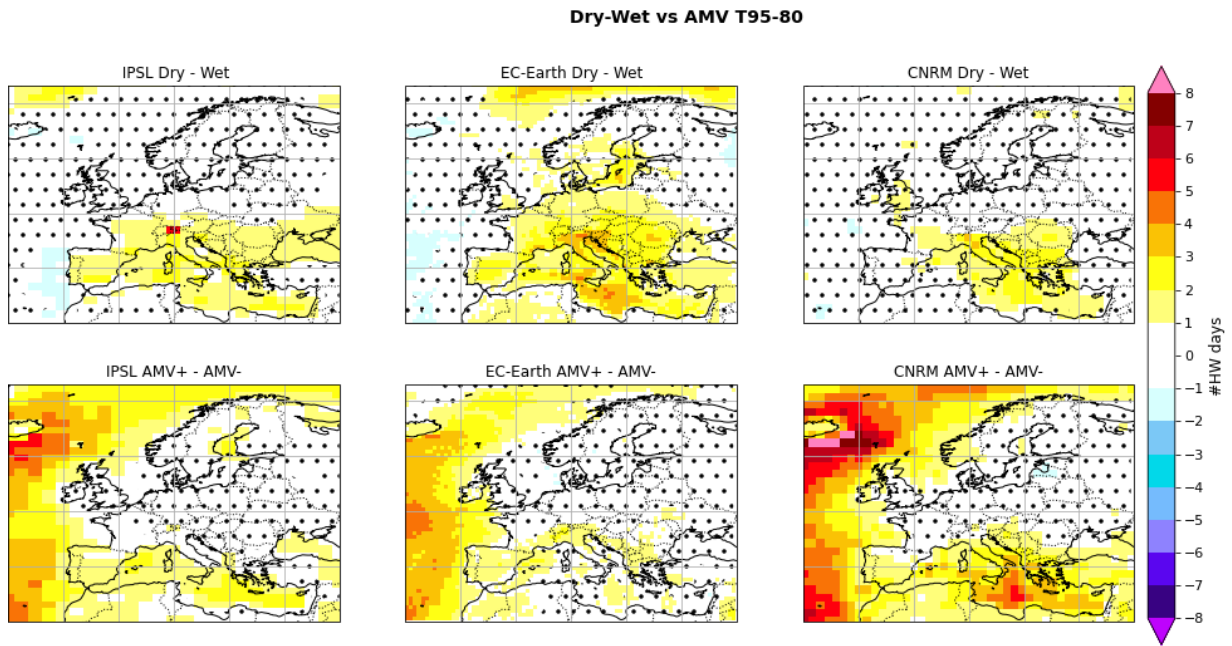


Figure 9: *Mean anomaly maps for the threshold based definition, with thresholds T_1 and T_2 corresponding to the 95th and 80th percentile of the local JJA T_{max} distribution. The maps show the difference of the mean number of heatwaves days per year between (top line) the dry and the wet ensembles and (bottom line) the AMV+ and AMV- ensembles for each of the three models. Hatching denotes area below the 95% significance level according to a bootstrap test.*

of all differences between two distinct samples and compute the quantiles from the distribution. We consider the difference at each grid point to be significant at the 95% significance level whenever it is lower than the 0.025 quantile or higher than the 0.975 quantile.

A.2 Additional figures

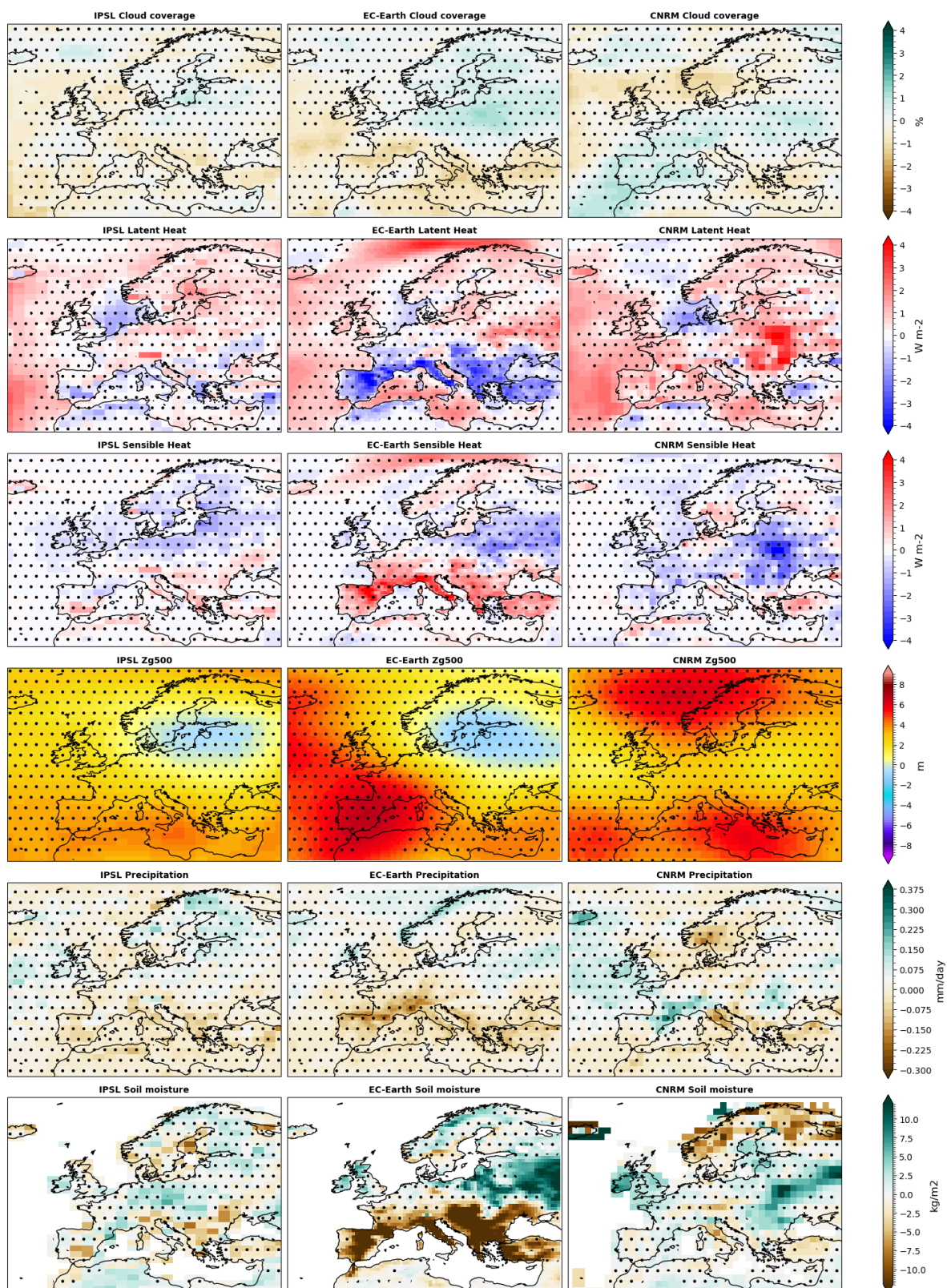


Figure 10: *Mean response maps to the AMV phase for different fields.* Each map represents the mean difference between AMV+ and AMV- of (from top to bottom row) percentage of cloud coverage, Latent heat, sensible heat, 500hPa geopotential height, precipitation, soil moisture. The average is taken with respect to the months of June, July and August. Each column represents a model. Stippling denotes area below the 95% significance level according to a bootstrap test

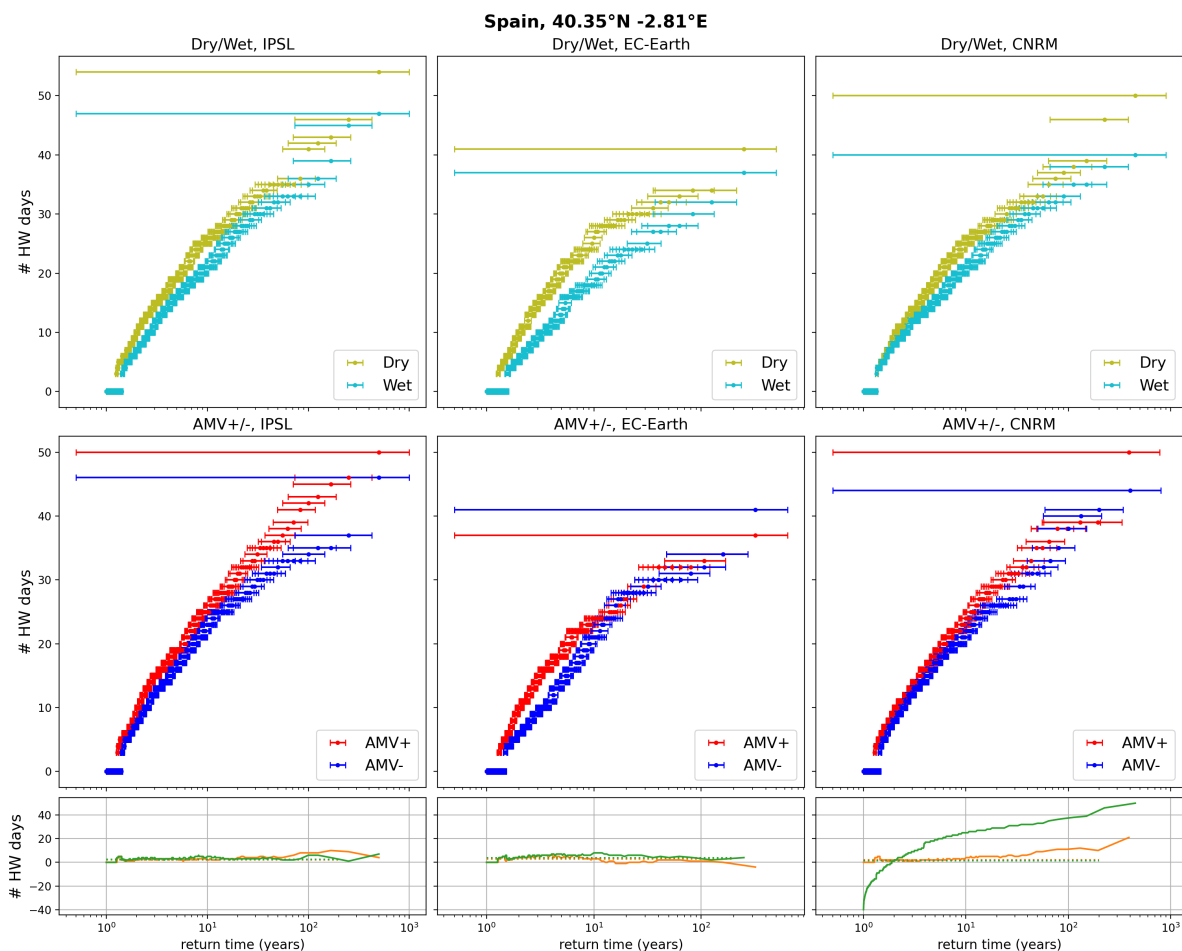


Figure 11: *Return time curves for the threshold based definition (section 2.3.1).* The plots show the yearly number of heatwave days as a function of the return time (in years) for Dry and Wet ensembles (top row) and for AMV+ and AMV- ensembles (bottom row) for the three models. Error bars correspond to one standard deviation of the estimated return time needed to observe an event of a certain amplitude. The third row shows the Dry - Wet (green) and AMV+ - AMV- (orange) differences as a function of the return time. The dotted lines indicate the mean difference values. For each model the chosen grid point covers the coordinate indicated in the figure title which corresponds to a location in the Northeast of Spain, close to the Mediterranean Sea.

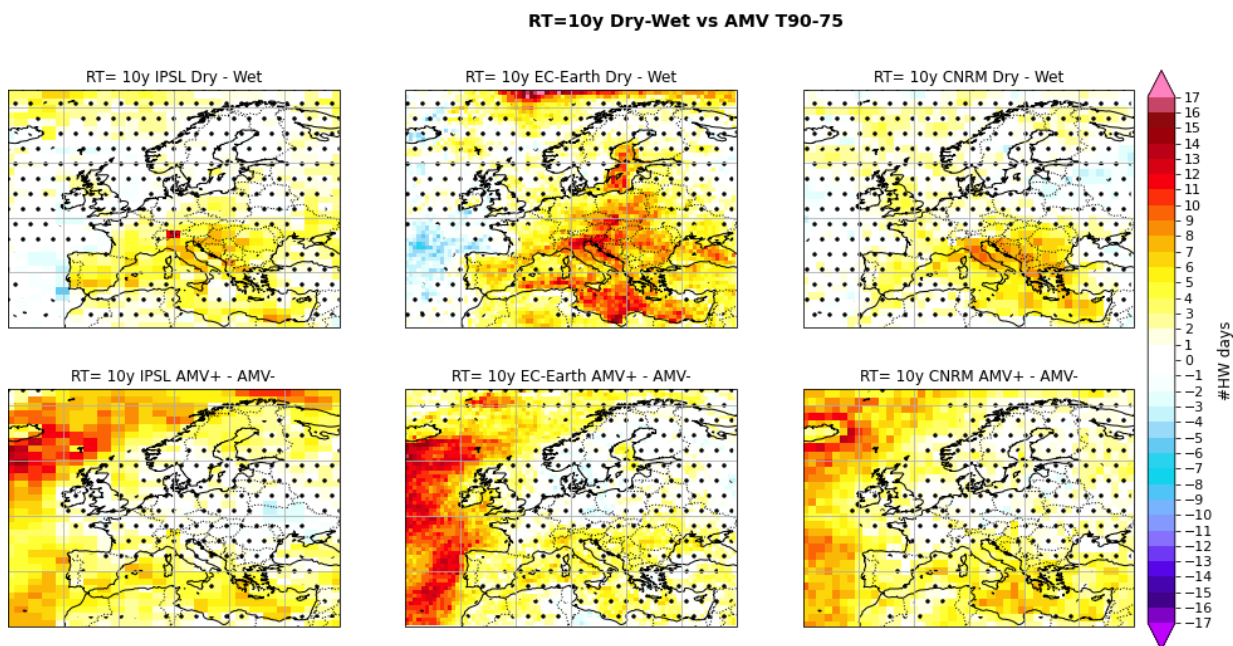


Figure 12: *10 years return time maps for the threshold based definition.* The maps show the yearly heatwaves days difference between (top line) the dry and wet ensembles and (bottom line) the AMV+ and AMV- ensembles, conditioned over the return time of 10 years. Stippling denotes area below the 95% significance level according to a bootstrap test.

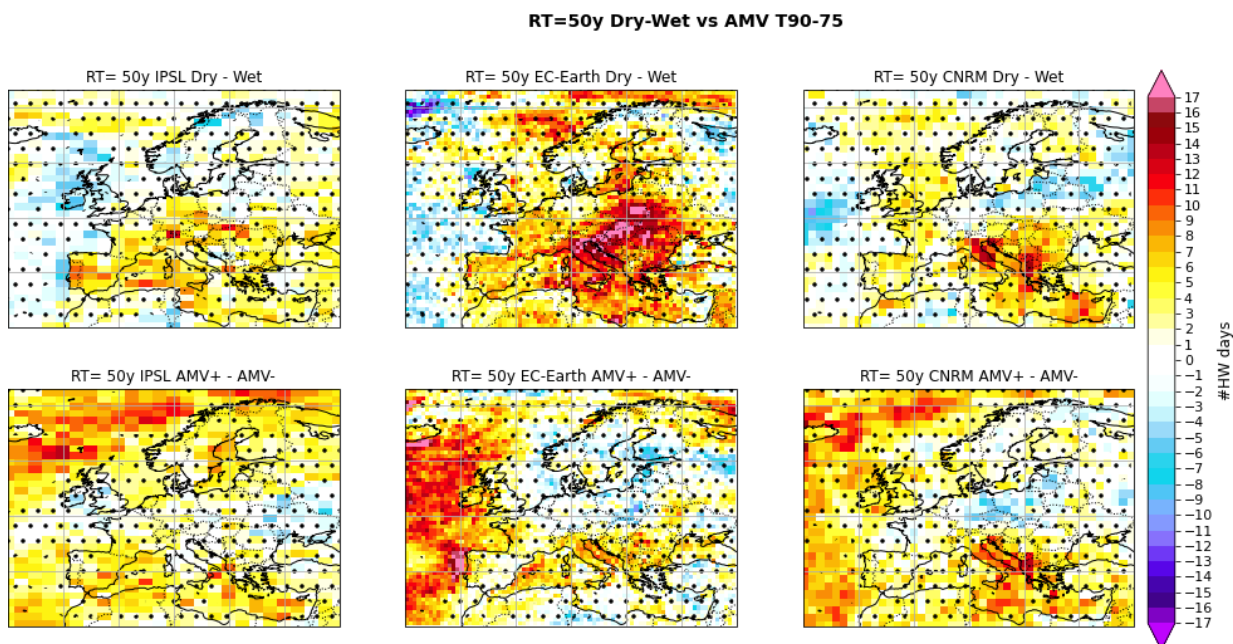


Figure 13: *50 years return time maps for the threshold based definition.* The maps show the yearly heatwaves days difference between (top line) the dry and wet ensembles and (bottom line) the AMV+ and AMV- ensembles, conditioned over the return time of 50 years. Stippling denotes area below the 95% significance level according to a bootstrap test.